SciEn

Proceedings of 8th International Conference on Mechanical Engineering and Renewable Energy 2025
10-12 December, 2025, Chattogram, BANGLADESH

SciEn Conference Series: Engineering Vol. 4, 2026, pp 68-72 https://doi.org/10.38032/scse.2026.4.40

Design and Optimization of Lead-Free Chalcogenide Perovskite Solar Cells: 30.64% Efficiency with $MgHfS_3$ Absorber

*Omkar Chowdhury**, *Utsa Bhowmik*

Department of Electrical and Electronic Engineering, CUET, Chattogram-4349, Bangladesh

ABSTRACT

This study presents a numerical simulation of an inorganic, lead-absent chalcogenide perovskite with the configuration FTO/ZrS_2/$MgHfS_3$/SnS/Pt, utilizing the SCAPS-1D simulator. The device employs $MgHfS_3$ as the absorber layer due to its promising bandgap of 1.43 eV and enhanced moisture stability. The effects of light-harvesting layer thickness and doping levels of the electron transport layer (ZrS_2) and hole transport layer (SnS) were systematically investigated to optimize photovoltaic performance. The results demonstrate that an absorber thickness of 1.1 µm and doping concentrations of 10^{19} cm^{-3} for both ETL and HTL yield a maximum power conversion efficiency of 30.64% at a defect density of 10^{15} cm^{-3}, with an open-circuit voltage (V_{OC}) of 1.1611 V, short-circuit current density (J_{SC}) of 31.19 mA/cm^2, and fill factor (FF) of 84.6%. The impact of operating temperature was also analyzed, revealing a slight decline in performance with increasing temperature. These findings highlight the potential of $MgHfS_3$-based chalcogenide perovskite solar cells as a stable and efficient alternative to conventional perovskite solar cells, offering a pathway toward sustainable and high-performance photovoltaic technology.

.

Keywords: Chalcogenide, Perovskite, SCAPS-1D, $MgHfS_3$

1. Introduction

Solar cells represent a vital renewable energy technology, converting sunlight directly into electricity and offering a clean, sustainable alternative to fossil fuels, which significantly contribute to greenhouse gas emissions. Solar power addresses the rising global energy demand while maintaining environmental sustainability. Conventional silicon-based solar cells have attained efficiencies of up to 29% [1], yet their production involves costly and energy-intensive processes, such as the Czochralski method for creating high-purity crystalline silicon wafers, which increases their carbon footprint and diminishes the ecological advantages of solar energy [2]. To address these issues, researchers are exploring advanced materials like perovskites. Organic-inorganic perovskite solar cells (PSCs) have gained prominence over traditional silicon cells due to their adjustable bandgaps, low-temperature fabrication, cost-effective production, and lightweight, flexible properties. Remarkably, the power conversion efficiency (PCE) of n-i-p type perovskite photovoltaic devices has grown from 3.8% to 25.2% in just ten years, establishing them as a strong contender to silicon-based solar cells. [3]. Despite achieving high efficiencies, the large-scale adoption of PSCs is limited by ongoing issues such as lead toxicity, phase instability, ion migration, and susceptibility to environmental degradation from moisture, heat, and ultraviolet (UV) exposure [4,5]. Thus, chalcogenide perovskite material $MgHfS_3$ can be a promising choice as it has more air and moisture stability [6]. Given shortcomings of current lead-free absorbers in combining high efficiency, defect tolerance, and phase stability, a new materials class is needed. Chalcogenide perovskites (ABX_3, X = S, Se, Te) are a promising candidate: they retain the advantageous perovskite crystal framework while their strong covalent metal–chalcogen bonds reduce ion migration and improve environmental stability compared with halide perovskites [8]. Figure 1 shows the standard CP structure.

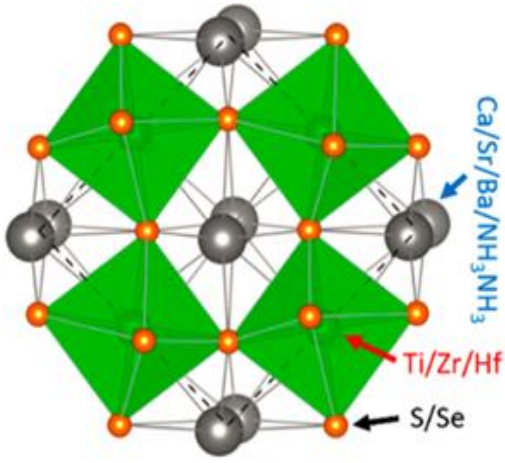

Fig. 1: A standard chalcogenide perovskite (CP) structure designed for application in solar energy systems [7].

Various chalcogenide perovskites (CPs) including $BaZrS_3$, $CaZrS_3$, $SrTiS_3$, and $CaSnS_3$ have been experimentally studied to evaluate their suitability for solar cell applications. Additionally, CPs like $BaZrS_3$, $SrZrS_3$, $BaHfS_3$, $SrHfS_3$,

* Corresponding Author Email Address: u1902138@student.cuet.ac.bd Published By: SciEn Publishing Group

$CaZrS_3$, and $CaHfS_3$ exhibit perovskite-type structures with optimal bandgaps for photovoltaic use. Theoretical studies indicate that CPs possess higher excitonic binding energies than lead-halide perovskites, and their bandgap and absorption coefficient, as determined by Spectroscopic Limited Maximum Efficiency (SLME), highlight their potential as highly effective solar cell absorbers [9].

Balogun et al. recently used density-functional-theory (DFT) to examine the optoelectronic properties of the chalcogenide perovskite $MgHfS_3$, focusing on its bandgap, absorption spectra, and non-radiative recombination losses. They reported a direct bandgap of 1.43 eV and an absorption coefficient of 4.9×10^8 m^{-1} [10]. Therefore, $MgHfS_3$ in this work is treated as a predicted chalcogenide-perovskite candidate primarily explored by first-principles calculations. Previous DFT studies specifically on $MgHfS_3$ report favorable formation energetics and strong optical absorption consistent with a stable absorber candidate. To date, experimental thin-film photovoltaic demonstrations of $MgHfS_3$ have not been reported in the literature, and consequently the present results are predictive in nature. [10]. With a bandgap close to the ideal for single-junction solar cells, $MgHfS_3$ shows considerable promise as an efficient photovoltaic absorber, providing the basis for this study. More recently, Feika et al. modeled an $MgHfS_3$-based perovskite photovoltaic device with an $FTO/TiO_2/MgHfS_3/Cu_2O/Au$ configuration using SCAPS-1D, achieving an optimized efficiency of 27.61% by varying the absorber thickness, defect densities, and interface properties [9].In this prior work where numerical modeling of an $MgHfS_3$-based perovskite solar cell TiO_2 serves as the electron transport layer (ETL) and Cu_2O as the hole transport layer (HTL).

This study utilized SCAPS-1D to simulate an inorganic, lead-free $MgHfS_3$-based chalcogenide perovskite solar cell. The device was modeled with a $FTO/ZrS_2/MgHfS_3/SnS/Pt$ configuration, considering both standard and N-I-P structures. To enhance performance, the absorber thickness and levels of doping of the ETL and HTL were altered. Maximum efficiency was obtained with the optimized $FTO/ZrS_2/MgHfS_3/SnS/Pt$ structure..

2. Methodology

2.1 Simulation model

Simulation is a useful method for visualizing how a solar cell works and testing whether a proposed design is practical. It permits scientists to rapidly review a photovoltaic device's output and observe how various component factors impact its operation without the prolonged durations or substantial expenses of building actual prototypes. Multiple programs exist for photovoltaic device modeling, such as SCAPS-1D, wxAMPS-1D, and Silvaco-TCAD [11]. In this research, a 1D n-i-p flat heterojunction perovskite setup ($FTO/ZrS_2/MgHfS_3/SnS/Pt$) was modeled with SCAPS-1D (v3.3.10), software created at Ghent University, Belgium. This software determines energy level schematics, charge carrier levels, J-V profiles, alternating current reactions, and light reactions by addressing core semiconductor formulas, like Poisson's equation and continuity formulas for electrons and holes [12]. All modeling occurred under standard AM 1.5G light (100 mW/cm^2) at 300 K, ignoring light bounce at layer boundaries or exteriors. The setup was simulated solely in an n-i-p format with $FTO/ZrS_2/MgHfS_3/SnS/Pt$ arrangement, since initial modeling showed better output than p-i-n versions. To boost output, the light-harvesting thickness and concentrations of doping of the ETL and HTL were adjusted. The top efficiency was attained with the improved $FTO/ZrS_2/MgHfS_3/SnS/Pt$ layout.

2.2 Device structure

In the planned device layout (Fig. 2), SnS acts as the hole carrier layer, whereas $MgHfS_3$ is the targeted perovskite light harvester. ZrS_2 functions as the electron carrier layer, and FTO functions as the transparent conductive oxide (TCO). Pt is chosen as the rear contact. The HTL's primary function is to effectively draw holes from the light harvester and move them to the rear contact [13]. The absorber, a perovskite material, forms the central component of the solar cell, capturing sunlight and generating charge carriers. The ETL is tasked with collecting and transporting electrons once they are injected from the absorber [14]. Positioned at the cell's front, the TCO enables incident sunlight to penetrate the absorber while conducting separated electrons to the external circuit.

In this setup, FTO is preferred as the TCO due to its high electrical conductivity ($10^4 \Omega^{-1} \cdot cm^{-1}$), excellent optical transmission (>80%), low refractive index, and robust stability and durability [15].

.

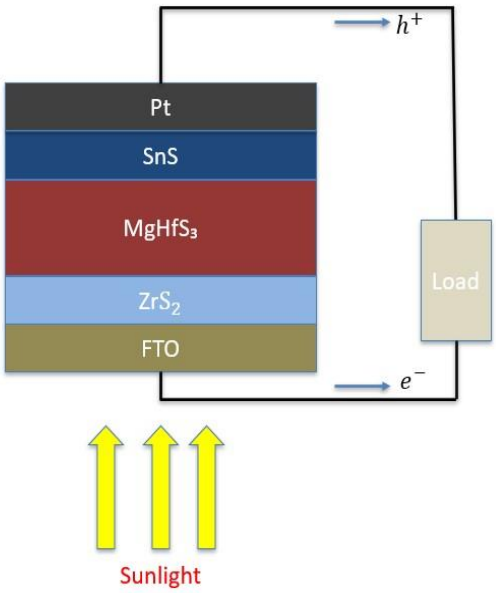

Fig. 2: Schematic representation of the proposed n–i–p chalcogenide perovskite solar cell

2.3 Optoelectronic properties and defects

The light absorption rates for various layers were calculated using the standard SCAPS light absorption method with a square root sub-method. The optical bandgap, carrier mobilities, electron affinity, and other key parameters for each layer were compiled from previously reported experimental and theoretical sources, as detailed in Table 1.Interface defect parameters for the ETL/CPs and CPs/HTL junctions are presented in Table 2 [9,16,17,18]. The thermal velocities of both electrons and holes were set to 1×10^7 $cm.s^{-1}$, while the work function of Pt is 5.7 eV which functions as the back contact. Defects are modeled as neutral traps with

Shockley-Read-Hall (SRH) recombination, using a bulk density of 10^{15} cm^{-3} (low for optimized perovskites). However, the 1D SCAPS model does not fully capture grain boundary (GB) effects in polycrystalline films, which introduce deep traps and can reduce carrier diffusion lengths, potentially slashing PCE in real devices. Interface recombination is included via surface densities of 10^{12} cm^{-3}, but assumes uniform junctions without lattice mismatch traps.

Table1: Initial parameters of all layers in the optimized configuration

Parameter	FTO	ZrS_2	$MgHfS_3$	SnS
Thickness (nm)	10	20	1100	100
Bandgap energy Eg (eV)	3.5	2.500	1.43	1.3
Electron Affinity (eV)	4	4.100	4.1	4.2
Relative permittivity, μ_r	9	16.4	9.6	12.6
Density of states of CB, N_c (cm^{-3})	2.2E+18	2.2E+18	2.2E+18	2.2E+18
Density of states of VB, N_v (cm^{-3})	1.8E+19	1.8E+19	1.8E+19	1.8E+10
Thermal velocity of e^-, v_n (cm/s)	1.0E+7	1.0E+7	1.0E+7	1.0E+7
Thermal velocity of h^+, v_p (cm/s)	1.0E+7	1.0E+7	1.0E+7	1.0E+7
Mobility of e^-, μ_n (cm^2 V^{-1} s^{-1})	2E+1	2.3E+3	1.7E-2	1.0E+2
Mobility of h+, μ_p (cm^2 V^{-1} s^{-1})	1E+1	1.3E+3	5.9E-2	4.0E+0
Donor density, N_D (cm^{-3})	1.0E+18	1.0E+19	1.0E+12	0
Acceptor density, N_A (cm^{-3})	0	0	1.0E+12	1.0E+19
Total Defect density, N_t (cr	1.0E+15	1.0E+15	1.0E+15	1.0E+15
References	[16]	[17]	[9]	[18]

Table 2: Properties of the interface defect layer

Parameters	ETL/Absorber	Absorber/HTL
Defect type	Neutral	Neutral
Electron Capture Area (cm^2)	10^{-15}	10^{-18}
Hole Capture Area (cm^2)	10^{-15}	10^{-16}
Energetic distribution	Single	Single
Benchmark for defect energy position (E^t)	Over the topmost Valence Band Edge	Over the topmost Valence Band Edge
Energy relative to benchmark (eV)	0.6	0.05
Total defect ($1/cm^3$)	10^{12}	10^{12}

3. Results and Discussion

3.1 Impact of absorber layer thickness

The absorber layer thickness is a key factor influencing the device performance. In this research, it was adjusted from 0.1 µm to 1.5 µm, with HTL and ETL thicknesses fixed at 0.1 µm and 0.02 µm, respectively. Fig. 3 presents the associated shifts in all four solar cell parameters. As the absorber thickness increases, V_{OC} and J_{SC} both rise, whereas FF shows a slight reduction. The efficiency increases with absorber thickness up to 1.1 µm due to better photon absorption and more electron-hole pair generation. Beyond this, it plateaus until 1.5 µm, then drops as thicker layers cause more carrier recombination from longer travel paths [19].

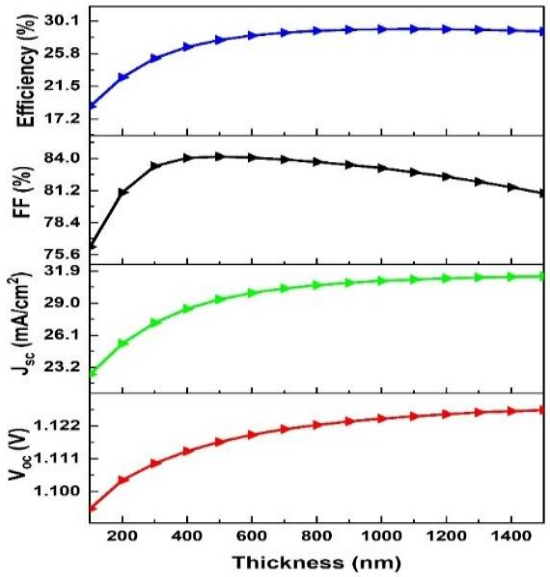

Fig. 3: Effect of light harvesting layer thickness changes on the device's output

3.2 Impact of doping concentration of HTL (NA)

The hole carrier layer (HTL), positioned between the perovskite and metal electrode, improves photovoltaic device output by effectively pulling holes from the light-

harvester and moving them to the electrode while blocking electrons from the anode. Furthermore, the HTL aids device reliability by guarding against humidity and lessening wear and rust [20]. Doping the HTL is essential, as the doping level greatly affects photovoltaic device output. In this research, the SnS doping level(N_A) was adjusted from 10^{16} cm^{-3} to 10^{20} cm^{-3}, while the ZrS_2 doping remained fixed at 10^{18} cm^{-3} . Fig. 4 demonstrates how the photovoltaic device factors react to SnS doping changes. Outcomes show that J_{SC}, FF, and efficiency increase with higher N_A, whereas V_{OC} remains nearly constant. The highest efficiency, 29.65%, is achieved at $N_A = 10^{20}$ cm^{-3} for the FTO/ZrS_2/$MgHfS_3$/SnS/Pt structure. However, such a high doping concentration is challenging to realize experimentally, so 10^{19} cm^{-3} is chosen as the optimized doping for SnS.

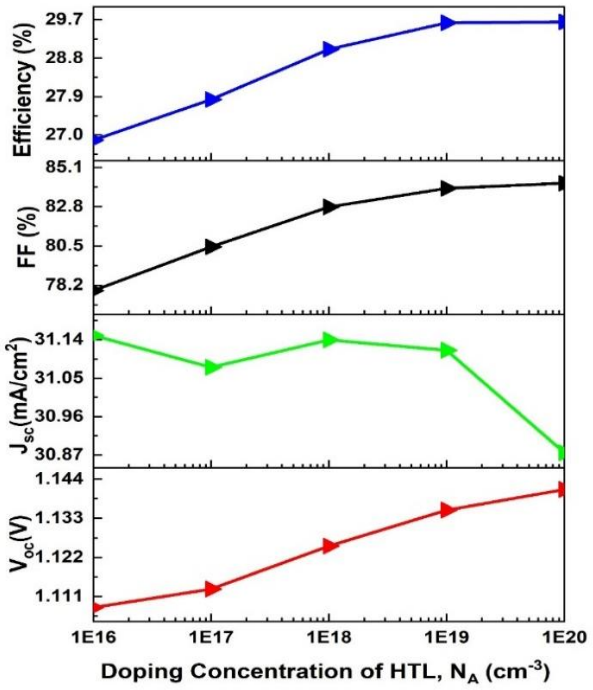

Fig. 4: Effect of the hole carrier layer doping level on solar factors

3.3 Impact of doping concentration of ETL (ND)

In perovskite solar cells, electron-hole pairs are separated at the absorber/ETL boundary, and the ETL transports electrons away from this layer, preventing recombination with holes in the perovskite [21]. In this research, the ZrS_2 doping level was adjusted from 10^{16} cm^{-3} to 10^{20} cm^{-3}, with SnS doping held at 10^{19} cm^{-3}. he impacts of N_D on device output are displayed in Fig. 5. Efficiency rises with N_D up to 10^{19} cm^{-3} and then levels off, with VOC remaining nearly constant, while FF and Jsc continue to rise. The optimal doping concentration of ZrS_2 is therefore 10^{19} cm^{-3}, at which the device achieves a maximum efficiency of 30.64%.

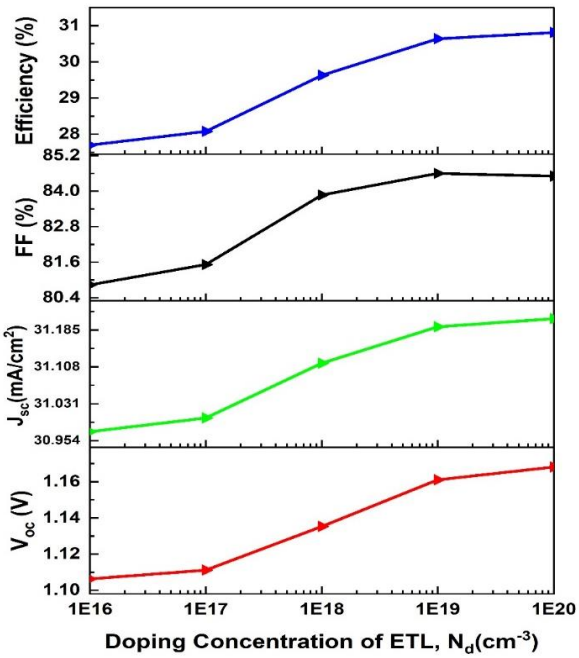

Fig. 5: Effect of the electron carrier layer doping level on solar factors

3.4 Impact of working temperature

As working temperature notably affects photovoltaic device output, models were run by changing temperature from 300 K to 400 K under steady 1-sun light, keeping other factors fixed. Fig. 6 displays the device's solar factor variations with temperature. It was noted that rising temperature led to a clear decrease in all PV factors except J_{SC}. Fig. 6: Graph illustrating PV factor changes with various operating temperatures.

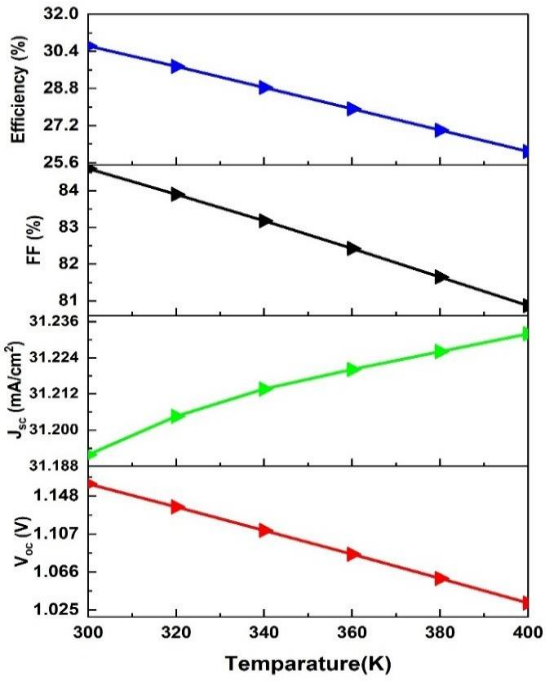

Fig. 6: Plot showing PV factor changes with various operating temperatures.

3.5 J-V profile of the photovoltaic device

The current density-voltage (J-V) traits of the optimized perovskite photovoltaic device are shown in Fig. 7. The curve exhibits standard diode behavior, with a sharp current density fall near the open-circuit voltage. Key photovoltaic parameters extracted from the curve include a V_{OC} of 1.1611 V, a J_{SC} of 31.19 mA/cm², a FF of 84.6%, and a maximum PCE of 30.64%. These results indicate excellent charge pulling and minimal recombination losses, confirming the effectiveness of the chosen material configuration and optimized doping concentrations in the device. The simulated PCE is sensitive to absorber quality — realistic increases in bulk/interface defect density or under-doping typically cut efficiency by ~10–20%, as shown in SCAPS studies [22].

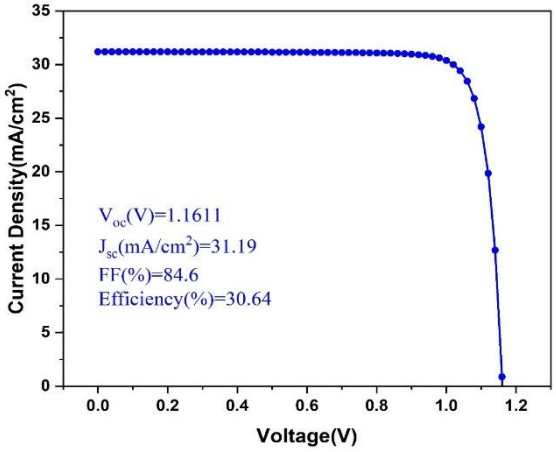

Fig. 7: J-V curve of the solar cell

3.6 Comparison with prior studies

Table 3: Performance Comparison Between Proposed and Reported $MgHfS_3$ Photovoltaic Devices

Device Structure	V_{oc} (volts)	J_{sc} (mA/cm^2)	FF (%)	PCE (%)	Ref
ITO/ZnO/$MgHfS_3$/Cu_2O/Au	1.2629	24.44	89.46	27.61	[9]
FTO/ZrS_2/$MgHfS_3$/SnS/Pt	1.1611	31.19	84.6	30.64	This Work

To evaluate performance, we compared our device against prior work (Table 3). The reference ITO/ZnO/$MgHfS_3$/Cu_2O/Au device reported V_{OC}=1.2629 V, J_{SC}=24.44 mA·cm^{-2}, FF = 89.46%, and PCE = 27.61% [9]; our FTO/ZrS_2/$MgHfS_3$/SnS/Pt design yields V_{OC}=1.1611V, J_{SC}=31.19 mA·cm^{-2}, FF = 84.6%, and PCE = 30.64%. The higher PCE is driven primarily by the substantially larger J_{SC} (improved absorption and collection) despite a modest drop in V_{OC} and FF, demonstrating the benefit of the modified ETL/HTL stack.

4. Conclusion

This research has effectively showcased the potential of $MgHfS_3$-based chalcogenide perovskite solar cells through numerical modeling with the SCAPS-1D simulator. The optimized FTO/ZrS_2/$MgHfS_3$/SnS/Pt device structure obtained a efficiency (PCE) of 30.64%. The simulated PCE of 30.64% approaches the Shockley-Queisser (SQ) radiative limit of around 33.0% for a 1.43 eV bandgap under AM 1.5G, representing ~93-95% of the theoretical maximum. This high value assumes radiative recombination dominance and ideal conditions. However, SCAPS-1D's assumptions—neglecting optical losses like reflectance, parasitic absorption , series and shunt resistances, and hysteresis—inflate performance. In practice, these could reduce J_{SC} and PCE aligning with certified perovskite records (~26%). The result motivates $MgHfS_3$ but underscores the need for experimental validation to confirm near-SQ potential. Moreover, the device achieves a V_{OC} of 1.1611 V, J_{SC} of 31.19 mA/cm², and FF of 84.6%, mainly because of improved photon absorption and charge collection enabled by ZrS_2 (ETL) and SnS (HTL). An optimal absorber thickness of 0.8–1.0 μm balances efficiency and recombination, confirming $MgHfS_3$ as a stable, lead-free candidate for next-generation photovoltaic development.

5. References

[1] Blakers, A. and Zin, N., 2013. High efficiency silicon solar cells. *Energy Procedia*, 33, pp.1–10.

[2] Benick, J. and Hoex, J., 2008. High efficiency n-type Si solar cells on Al_2O_3-passivated surfaces. *Applied Physics Letters*, 92(25), pp.253504-1–253504-3.

[3] Kojima, A., Teshima, K., Shirai, Y. and Miyasaka, T., 2009. Organometal halide perovskites as visible-light sensitizers for photovoltaic cells. *Journal of the American Chemical Society*, 131(17), pp.6050–6051.

[4] Zheng, Y. and Yang, S., 2022. Stabilization techniques of lead halide perovskite for photovoltaic applications. *Solar RRL*, 6(1), p.2100710.

[5] Babayigit, A., Ethirajan, A., Muller, M. and Conings, B., 2016. Toxicity of organometal halide perovskite solar cells. *Nature Materials*, 15(3), pp.247–251.

[6] Nishigaki, Y. et al., 2020. Extraordinary strong band-edge absorption in distorted chalcogenide perovskites. *Solar RRL*, 4(5), p.1900555.

[7] Sun, Y.-Y., Agiorgousis, M. L., Zhang, P. and Zhang, S., 2015. Chalcogenide perovskites for photovoltaics. *Nano Letters*, 15(1), pp.581–585.

[8] Njema, G. G. and Kibet, J. K., 2025. A review of chalcogenide-based perovskites as the next novel materials: Solar cell and optoelectronic applications, catalysis and future perspectives. *Next Nanotechnology*, 7, p.100102.

[9] Adewoyin, A. D., Feika, A. M., Olopade, M. A. and Oyebola, O. O., 2024. Performance optimization of $MgHfS_3$ chalcogenide perovskite solar cells using SCAPS-1D. *East European Journal of Physics*, (3), pp.456–464.

[10] Balogun, R. O., Olopade, M. A., Oyebola, O. O. and Adewoyin, A. D., 2021. First-principles calculations to investigate structural, electronic and optical properties of $MgHfS_3$. *Materials Science and Engineering B*, 273, p.115405.

[11] Khatoon, S. et al., 2022. Design of a $CH_3NH_3PbI_3$/$CsPbI_3$-based bilayer solar cell using device simulation. *Heliyon*, 8(7), p.e09941.

[12] Burgelman, M., Nollet, P. and Degrave, S., 2000. Modelling polycrystalline semiconductor solar cells. *Thin Solid Films*, 361–362, pp.527–532.

[13] Igbari, F. et al., 2016. A room-temperature $CuAlO_2$ hole interfacial layer for efficient and stable planar perovskite solar cells. *Journal of Materials Chemistry A*, 4(4), pp.1326–1335.

[14] Yu, M. et al., 2020. The influence of the electron transport layer on charge dynamics and trap-state properties in planar perovskite solar cells. *RSC Advances*, 10(21), pp.12347–12353.

[15] Chavan, G. T. et al., 2023. A brief review of transparent conducting oxides (TCO): The influence of different deposition techniques on the efficiency of solar cells. *Nanomaterials*, 13(7), p.1226.

[16] Alipour, H. and Ghadimi, A., 2021. Optimization of lead-free perovskite solar cells in normal structure with WO_3 and water-free PEDOT:PSS composite for hole transport layer by SCAPS-1D simulation. *Optical Materials*, 120, p.111432.

[17] Arockiya-Dass, K. T., Sekar, K. and Marasamy, L., 2023. Theoretical insights of degenerate ZrS_2 as a new buffer for highly efficient emerging thin-film solar cells. *Energy Technology*, 11(10), p.2300333.

[18] Basak, A. and Singh, U. P., 2021. Numerical modelling and analysis of earth-abundant Sb_2S_3 and Sb_2Se_3 based solar cells using SCAPS-1D. *Solar Energy Materials and Solar Cells*, 230, p.111184.

[19] Ouslimane, T. et al., 2021. Impact of absorber layer thickness, defect density and operating temperature on the performance of $MAPbI_3$ solar cells based on ZnO electron transporting material. *Heliyon*, 7(3), p.e06379.

[20] Li, S. et al., 2021. A brief review of hole transporting materials commonly used in perovskite solar cells. *Rare Metals*, 40(10), pp.2712–2729.

[21] Kim, T., Lim, J. and Song, S., 2020. Recent progress and challenges of electron transport layers in organic–inorganic perovskite solar cells. *Energies*, 13(21), p.5572.

[22] Taheri, S., Minbashi, M. and Hajjiah, A., 2021. Effect of defects on high efficient perovskite solar cells. *Optical Materials*, 111, p.110601.